LAWRENCE
LIVERMORE
NATIONAL
LABORATORY

LLNL-CONF-864568

Modifying X-ray Streak Cameras for Operation on Igniting Fusion Experiments

S. F. Khan, P. R. Nyholm, K. J. Decker, A. G. MacPhee, T. R. Hilsabeck, D. Boyle, N. Palmer, T. A. Miller, A. C. Carpenter

May 17, 2024

25th Topical Conference on High Temperature Plasma Diagnostics
Asheville, NC, United States
April 21, 2024 through April 25, 2024

Disclaimer

Modifying X-ray Streak Cameras for Operation on Igniting Fusion Experiments

S. F. Khan[1], P. R. Nyholm[1], K. J. Decker[1], A. G. MacPhee[1], T. R. Hilsabeck[1], D. Boyle[1], N. Palmer[1], T. A. Miller[1, 2], A. C. Carpenter[1]

[1]*Lawrence Livermore National Laboratory, Livermore, CA 94550, USA*
[2]*General Atomics, San Diego, CA 92186, USA*

(Presented XXXXX; received XXXXX; accepted XXXXX; published online XXXXX)
The National Ignition Facility produced the first nuclear fusion experiment demonstrating net positive energy gain on December 5th, 2022. The X-ray streak camera that measures the bang time and burn-width from this landmark experiment had an electronic failure and did not record data. The CCD sensor was replaced with a radiation hardened CMOS sensor that has since demonstrated successful operation on repeat Ignition shots. Concurrently, an instrument artifact was identified that occurs when the signal consists primarily of energetic x-rays > 15 keV (common on burning plasma experiments). This artifact, which appears as a background pedestal, arises from the back x-ray fluorescence generated by the solid metal accelerating mesh behind the photocathode in the streak tube. We have mitigated this background signal by limiting the sensitive area of the photocathode. Herein, the details of the modifications and the results are presented.

I. INTRODUCTION

X-ray streak cameras are used in various fields[1–5] to measure the time history of X-rays emitted during experiments. At the National Ignition Facility[6] (NIF), X-ray streak cameras are used to track shell trajectories during implosions, spectrally resolve back-lighter signals, and determine the time and duration of the self-emitting core within Inertially Confined Fusion[7] (ICF) processes. With higher energy gain in ICF experiments, the diagnostic environment becomes challenging from the increase in neutrons, gamma rays and X-rays created. The diagnostics at the NIF have had to quickly transfer to radiation hardened components and add additional filtering so that usable data can continue to be collected during experiments.

We modified the X-ray streak camera called the SPIDER[5] which was designed to primarily measure the peak time of the hot spot emission, bang-time (BT), and the hot spot burn-width (BW). In ICF experiments, the BT gives information about the implosion velocity and the BW is related to the compression time. The SPIDER uses a fixed port at NIF coordinates (θ, φ) = (7°, 90°). It is located outside the target chamber about ~9.2 m from target chamber center. Thick neutron and Gamma ray shielding[5] has allowed it to successfully operate up to about 2 MJ yield. With a CsI photocathode and fixed filtering, the SPIDER is sensitive to x-rays between 6 keV to ~50 keV. Its temporal resolution is about 8 ps with the current 150 μm slit and using the fastest sweep mode (~1.3 ns total record). An example of data from the SPIDER is shown in Fig 1a). The instrument can be outfitted with different filters across the photocathode, usually two to three different thicknesses of titanium filters. The BT and BW are measured from the averaged lineouts from each channel (Fig. 1b).

Two independent modifications were made on the SPIDER to (1) allow the instrument to function in a higher neutron yield (5 MJ) environment and (2) enable measurements with harder x-rays without the accompanying background signal.

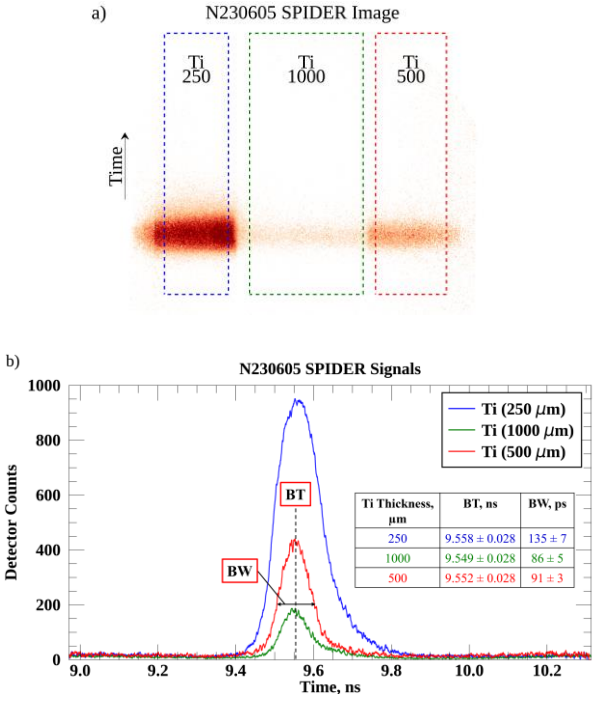

[a)]Author to whom correspondence should be addressed: khan9@llnl.gov

Fig. 1: a) Example SPIDER data from NIF shot # N230605 which used the triple Ti filter set: {250 µm, 1000 µm, 500 µm}. b) Averaged lineouts from the three Ti channels. The thinner filtered channels include the softer outgoing shock signal[8], so the BT is slightly later and BW larger.

II. UPGRADE FOR HIGH YIELD ENVIRONMENT

The CCD camera in SPIDER had an electronic failure and did not record data on the first fusion experiment[9–11] (Shot # N221204, yield = 3.15 MJ) with target energy gain > 1 (the laser energy entering the hohlraum versus the total neutron energy emitted). Prior experiments showed signs of approaching the sensor limit with the neutron generated background counts exceeding one-fourth of the CCD full well capacity (Shot # N210808, yield = 1.33 MJ shown in Fig. 2). Scaling this shot to the N221204 yield, we would expect a neutron floor background of ~40k counts which would still leave ~25k counts for the x-ray signals so the failure on N221204 was unexpected.

The CCD camera during the above shots was a Spectral Instruments SI-1000 with a Kodak KAF16801E sensor. We replaced the camera with a Spectral Instruments SI-1600S with a CIS-54[12] radiation hardened CMOS sensor. Only the necessary components of the CIS-54 camera are located in the radiation environment, the HTTP server controls for the camera are located outside the chamber and are connected via fiber optic cables. With this dump and read format the components requiring extra shielding are minimized.

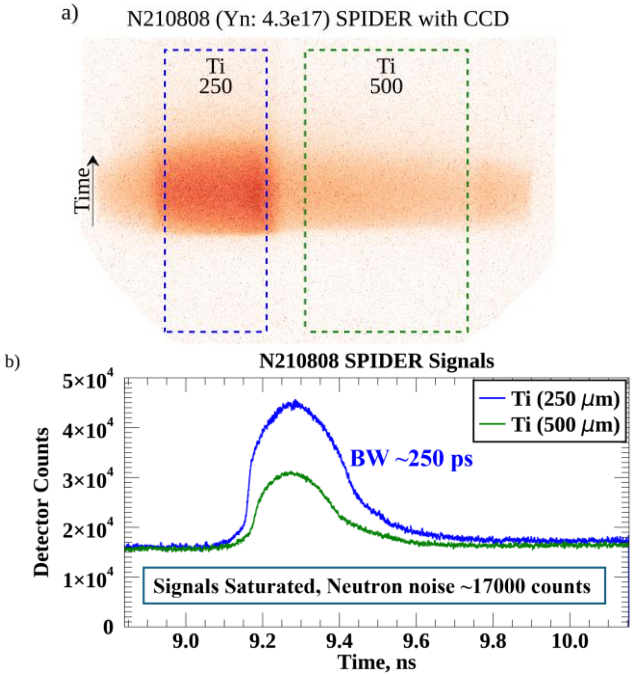

Fig. 2: a) SPIDER data from N210808 shows a significant neutron noise floor of ~17k counts (~1/4 the full well capacity). On top of that, the x-ray signal was too bright, and the record was broadened due to space charge spreading inside the streak tube. b) Burn width measured (~250 ps) is affected by both space charge broadening and MCP saturation.

This new camera, installed on 2/24/2023, allowed us to record data on experiments with yields above the previous failure. Data from the experiment, N231029 (Yield = 3.4 MJ), with yield exceeding the failure is shown in Fig. 3. The neutron background on the sensor was reduced to ~1800 counts and the S/N was excellent. We doubled the thickness of the titanium filters to reduce space charge broadening.

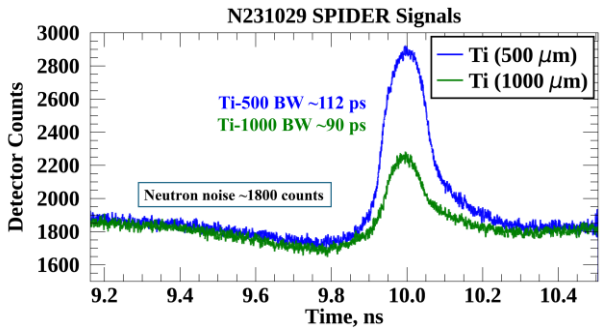

Fig. 3: SPIDER lineouts from N231029 (Yield = 3.4 MJ) using the new CIS-54 sensor shows good signal to noise and low neutron background.

III. THE X-RAY FLUORESCENCE PROBLEM

A. Source of the problem

X-ray Back Fluorescence is a problem on experiments with primarily high energy x-rays such as Igniting DT shots and shots utilizing the Advanced Radiographic Capability (ARC) laser system[13,14]. The origin of the x-ray back fluorescence is depicted in Fig. 4. A large portion of the experiment x-rays pass through the photocathode and irradiate the nickel accelerating mesh generating fluorescence x-rays that radiate in all directions. If the incoming x-rays are above the activation energy for the characteristic emission lines, x-ray fluorescence will be generated (> 7.5 keV for Ni). Some of the mesh generated x-rays travel back towards the photocathode and liberate additional photoelectrons that enter the streak tube and add to the experiment signal.

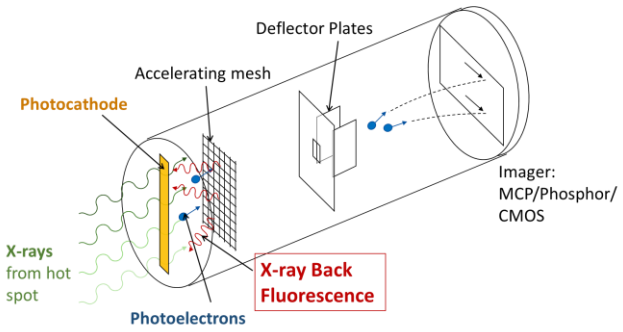

Fig. 4: Diagram of how a streak camera works. The X-ray back fluorescence is shown in red. X-rays (shown in green) from the experiment are converted to photoelectrons (shown as blue) in the photocathode which are accelerated using a potential difference at the metal accelerating mesh. However, a large portion of the experiment x-rays pass through the photocathode and activate fluorescence x-rays from the accelerating mesh. Some of these x-rays (shown in red) travel backwards to the photocathode and liberate more photoelectrons which also get accelerated in the streak tube and add to the SPIDER signal.

Evidence of the x-ray fluorescence is seen in the lineouts in N231029 (Fig. 3) but are better illustrated on an earlier experiment, N220109 (Fig. 5). The x-ray fluorescence signal looks like a rounded pedestal under the data. Comparing the self-emission signal (above the background) from the two channels, the counts in the 1000 µm Ti channel (green) should always be lower than the counts in the 500 µm Ti channel (blue) due to attenuation of the x-rays. However, the counts are about the same before and after the BT (circled in red in Fig 5.). According to hot spot models[15], it is not physically possible to have the same signal through both channels. The pedestal is shifted slightly later in time due to the 30° degree angle[5] of the incoming experiment x-rays and the time of flight difference between the photocathode and mesh (~13 ps).

The degree of the fluorescence pedestal varies from shot to shot and depends on the x-ray spectrum and filtering. The quantum efficiency of the CsI photocathode drops at higher x-ray energies so that less x-ray signal is converted to photoelectrons while relatively more fluorescence is generated. Therefore, this pedestal manifests itself in high performing ICF experiments or short pulse laser experiments (using ARC[13]). It is an artifact that can't be easily subtracted because the shape and amplitude of it requires knowing the full x-ray spectrum of the incoming x-rays. The pedestal heavily affects the BW measurement and any inference of the time-resolved electron temperature[15] of the hot spot. From the N220109 data, the BW measurement from the 1000 µm channel is about 50% greater than that from the 500 µm channel, contrary to simulations and analytical expectations. Removal of the background signal using polynomial fitting has been done but it gave inconsistent and unreliable results such as BW measurements much shorter than gamma ray measurements. The issue lies with the fact that the fluorescence signal depends on the time varying hot spot Temperature and brightness, making it difficult to model.

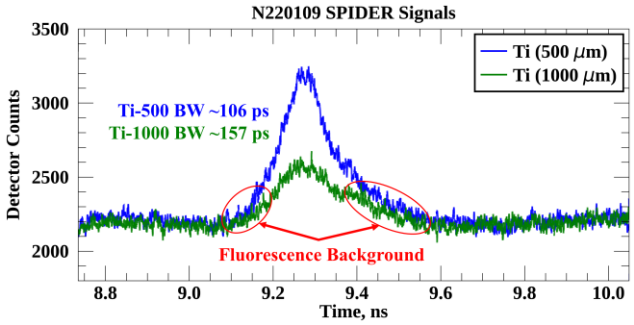

Fig. 5: SPIDER lineouts from N220109: the wings (circled in red) on the 1000 µm Ti signal is not real data, because it is not physically possible to have the same counts as that from the 500 µm thick Ti according to hot spot models.

B. Mitigation of the X-ray back fluorescence

We made two changes to mitigate the Fluorescence signal: (1) Replaced the Ni mesh with a plastic mesh with a thin high Z metal (gold) coating, reducing the x-ray fluorescence created and (2) Added a polyimide film aperture over the backside of the photocathode, which blocks most of the photoelectrons induced by the back fluorescence.

The Ni mesh was replaced on 11/20/2021 but it did not completely mitigate the x-ray fluorescence. A plastic mesh is expected to produce less fluorescence signal because the x-rays that are produced in its volume are lower energy and are mostly attenuated by the gold coating. The gold (~0.1 µm thick) creates x-ray fluorescence as well, but it should be much lower compared to the original Ni mesh (~15 µm thick) just due to the volume difference. The details of this mesh is not fully known except that it is a plastic mesh with gold coating as it was used on a legacy streak tube. A new gold coated plastic accelerating mesh has since been developed by General Atomics. A 1 mm thick graphite base is used instead of aluminum to further lower the x-ray fluorescence background. A 15 µm thick plastic mesh with 84% open area was produced by laser printing via two-photon polymerization process. A 100 nm layer of gold was applied by atomic layer deposition, but this thickness will likely be further reduced. Characterization and offline tests performed showed positive results. This new mesh will be deployed at the next opportunity.

The polyimide works (Fig 6.) by blocking the liberated photoelectron from the backside except for a small opening about the same size as the slit. The incoming experiment x-rays pass through a 150 µm slit at an incidence angle of 30° (30° incidence not depicted in Fig 6.) and create photoelectrons at the photocathode which are accelerated down the streak tube. The fluorescence x-rays created by the pass-through x-rays radiate backwards and, since the photocathode is greatly oversized (5 mm) compared to the front active width (150 µm), create electrons over a large

area. A thin film of 50 µm polyimide blocks the liberated electrons since they are born with sufficiently low energy of 7-10 eV (Monte Carlo simulations of CsI photocathode[16]). The stopping power of 50 µm thick polyimide is includes up to ~60 keV electrons[17].

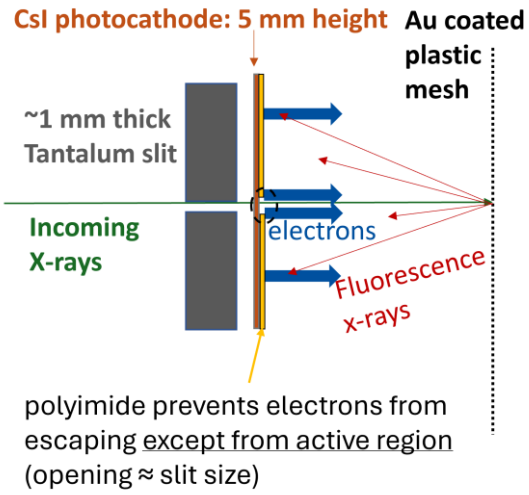

Fig. 6: Side view of photocathode and slit with polyimide shield. Experiment x-rays are limited to a 150 µm photocathode active area using a thick Ta aperture. Most of the x-rays pass through the photocathode and activate fluorescence x-rays that radiate isotropically. More photoelectrons are created from the entire backside of the photocathode (5 mm area). A layer of thin polyimide with a 300 µm opening around the slit opening mitigates the secondary photoelectron signal by about 15X.

SPIDER Data using this new polyimide shielded photocathode is shown in Fig. 7: N240210 (5.2 MJ) along with N231029 (3.4 MJ) showing a mostly mitigated pedestal. Since N240210 was a better performer, the x-ray spectrum would shift hotter, and we would expect more x-ray fluorescence relative to the hot spot emission signal. The recorded signal from N240210 shows a sharp rise and sharp fall of the emission compared to previous ICF DT shots. There is a small bump in the signal after the main emission due to imperfect background subtraction. In this new neutron environment, it appears that Cherenkov radiation is manifesting in the fiber-optic faceplate. The full 2-D SPIDER image shows a slightly higher background close to the edges of the imager with a gradual reduction towards the center.

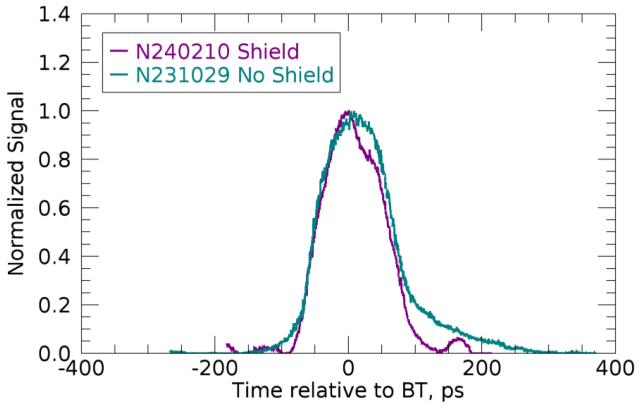

Fig. 7: Comparison of SPIDER lineouts from N240210 (with polyimide shield) and N231029 (without polyimide shield). The pedestal appears to have been mostly mitigated. There is a small bump in the signal after the main emission which is from imperfect background subtraction due to Cherenkov radiation in the fiber-optic imaging block.

IV. SUMMARY AND FUTURE

Replacing the CCD with a rad-hard CMOS allowed SPIDER to operate in our Ignition environment. Adding a Polyimide shield to block the photoelectrons from escaping the backside of the photocathode mitigated most of the Fluorescence artifact. In the future, other plastic meshes will be tested to try to eliminate the fluorescence signal. At higher yields, other issues are appearing: the X-rays produced are getting too bright and broadening the streaked record. One of the solutions we are pursuing is to replace the photocathode with the less sensitive KBr. The other issue is the Cherenkov radiation from the fiber-optic faceplate[5] that appears to have a circular structure. A long-term solution is to switch to a rad-hard direct electron detector instead of the CIS-54 sensor. This will allow us to remove the fiber-optic block and phosphor.

V. ACKNOWLEDGMENTS

The authors sincerely thank the NIF operations staff and the diagnostic leadership team who supported this work. This work was performed under the auspices of the U.S. Department of Energy by Lawrence Livermore National Laboratory under Contract No. DE-AC52-07NA27344. Release number: LLNL-CONF-864568.

VI. AUTHOR DECLARATIONS

A. Conflict of interest statement

The authors have no conflicts to disclose.

B. Author contributions

Shahab Khan: Conceptualization (equal); Formal Analysis (lead); Methodology (equal); Visualization (lead); Writing Draft (lead); Investigation (equal). **Peter Nyholm:** Conceptualization (equal); Methodology (equal); Resources (equal); Review & Editing (equal); Investigation (lead). **Kit Decker:** Review & Editing (equal); Investigation (equal). **Andrew MacPhee:** Conceptualization (equal); Methodology (equal); Review & Editing (equal). **Terry Hilsabeck:** Conceptualization (equal); Methodology (equal); Investigation (equal); Review & Editing (equal). **Dusty Boyle:** Review & Editing (equal); Resources (equal); Supervision (equal); Investigation (equal). **Nathan Palmer:** Conceptualization (equal); Methodology (equal); Review & Editing (equal). **Toby Miller:** Investigation (equal); Resources (equal); Review & Editing (equal).
Arthur Carpenter: Conceptualization (equal); Methodology (equal); Review & Editing (equal); Supervision (equal); Project Administration (lead).

VII. DATA AVAILABILITY

The data that support the findings of this study are available according to the data availability policy of Lawrence Livermore National Laboratory.

VIII. REFERENCES AND FOOTNOTES

[1] K.W. Hill, M. Bitter, L. Delgado-Aparicio, P.C. Efthimion, R. Ellis, L. Gao, J. Maddox, N.A. Pablant, M.B. Schneider, H. Chen, et. al., Rev. Sci. Instrum. **87**(11), 11E344 (2016).
[2] E.L. Dewald, O.L. Landen, L. Masse, D. Ho, Y. Ping, D. Thorn, N. Izumi, L. Berzak Hopkins, J. Kroll, A. Nikroo, and J.A. Koch, Rev. Sci. Instrum. **89**(10), 10G108 (2018).
[3] K.V. Cone, J. Dunn, M.B. Schneider, H.A. Baldis, G.V. Brown, J. Emig, D.L. James, M.J. May, J. Park, R. Shepherd, and K. Widmann, Rev. Sci. Instrum. **81**(10), 10E318 (2010).
[4] P.A. Jaanimagi, D.K. Bradley, J. Duff, G.G. Gregory, and M.C. Richardson, Rev. Sci. Instrum. **59**(8), 1854–1859 (1988).
[5] S.F. Khan, P.M. Bell, D.K. Bradley, S.R. Burns, J.R. Celeste, L.S. Dauffy, M.J. Eckart, M.A. Gerhard, C. Hagmann, D.I. Headley, et. al, *Target Diagn. Phys. Eng. Inert. Confin. Fusion*, (SPIE, 2012), pp. 33–40.
[6] G.H. Miller, E.I. Moses, and C.R. Wuest, Opt. Eng. **43**(12), 2841–2853 (2004).
[7] J. Lindl, Phys. Plasmas **2**(11), 3933–4024 (1995).
[8] A. Pak, L. Divol, G. Gregori, S. Weber, J. Atherton, R. Bennedetti, D.K. Bradley, D. Callahan, D.T. Casey, E. Dewald, T. Döppner, et. al., Phys. Plasmas **20**(5), 056315 (2013).
[9] The Indirect Drive ICF Collaboration, et. al., Phys. Rev. Lett. **132**(6), 065102 (2024).
[10] A. Pak, A.B. Zylstra, K.L. Baker, D.T. Casey, E. Dewald, L. Divol, M. Hohenberger, A.S. Moore, J.E. Ralph, D.J. Schlossberg, et. al., Phys. Rev. E **109**(2), 025203 (2024).
[11] A.L. Kritcher, A.B. Zylstra, C.R. Weber, O.A. Hurricane, D.A. Callahan, D.S. Clark, L. Divol, D.E. Hinkel, K. Humbird, O. Jones, et. al., Phys. Rev. E **109**(2), 025204 (2024).
[12] J. Prince, D. Hargrove, A. Carpenter, and G. Sims, *Hard X-Ray Gamma-Ray Neutron Detect. Phys. XXV*, (SPIE, 2023), pp. 90–103.
[13] J.M.D. Nicola, S.T. Yang, C.D. Boley, J.K. Crane, J.E. Heebner, T.M. Spinka, P. Arnold, C.P.J. Barty, M.W. Bowers, T.S. Budge, et. al., *High Power Lasers Fusion Res. III*, (SPIE, 2015), pp. 122–133.
[14] H. Chen, M.R. Hermann, D.H. Kalantar, D.A. Martinez, P. Di Nicola, R. Tommasini, O.L. Landen, D. Alessi, M. Bowers, D. Browning, et. al., Phys. Plasmas **24**(3), 033112 (2017).
[15] S.F. Khan, L.C. Jarrott, P.K. Patel, N. Izumi, T. Ma, A.G. MacPhee, B. Hatch, O.L. Landen, J. Heinmiller, J.D. Kilkenny, and D.K. Bradley, Rev. Sci. Instrum. **89**(10), 10K117 (2018).
[16] S.F. Khan, J.J. Lee, N. Izumi, B. Hatch, G.K. Larsen, A.G. MacPhee, J.R. Kimbrough, J.P. Holder, M.J. Haugh, Y.P. Opachich, P.M. Bell, and D.K. Bradley, *Target Diagn. Phys. Eng. Inert. Confin. Fusion II*, (SPIE, 2013), pp. 94–99.
[17] "Stopping-Power & Range Tables for Electrons, Protons, and Helium Ions," NIST, (2009).